ISSN 1063-7761, Journal of Experimental and Theoretical Physics, 2014, Vol. 118, No. 6, pp. 995–1011. © Pleiades Publishing, Inc., 2014.
Original Russian Text © M.Yu. Kagan, V.V. Val'kov, V.A. Mitskan, M.M. Korovushkin, 2014, published in Zhurnal Eksperimental'noi i Teoreticheskoi Fiziki, 2014, Vol. 145, No. 6, pp. 1127–1146.

REVIEW

The Kohn–Luttinger Effect and Anomalous Pairing in New Superconducting Systems and Graphene

M. Yu. Kagan[a,b], V. V. Val'kov[c], V. A. Mitskan[c,d], and M. M. Korovushkin[c]

[a] *Kapitza Institute of Physical Problems, Russian Academy of Sciences, Moscow, 119334 Russia*
[b] *Moscow State Institute of Electronics and Mathematics, National Research University Higher School of Economics, Moscow, 109028 Russia*
[c] *Kirensky Institute of Physics, Siberian Branch, Russian Academy of Sciences, Krasnoyarsk, 660036 Russia*
[d] *Reshetnev Siberian State Aerospace University, Krasnoyarsk, 660014 Russia*
e-mail: kagan@kapitza.ras.ru; vvv@iph.krasn.ru

Abstract—We present a review of theoretical investigations into the Kohn–Luttinger nonphonon superconductivity mechanism in various 3D and 2D repulsive electron systems described by the Fermi-gas, Hubbard, and Shubin–Vonsovsky models. Phase diagrams of the superconducting state are considered, including regions of anomalous *s*-, *p*-, and *d*-wave pairing. The possibility of a strong increase in the superconducting transition temperature T_c even for a low electron density is demonstrated by analyzing the spin-polarized case or the two-band situation. The Kohn–Luttinger theory explains or predicts superconductivity in various materials such as heterostructures and semimetals, superlattices and dichalcogenides, high-T_c superconductors and heavy-fermion systems, layered organic superconductors, and ultracold Fermi gases in magnetic traps. This theory also describes the anomalous electron transport and peculiar polaron effects in the normal state of these systems. The theory can be useful for explaining the origin of superconductivity and orbital currents (chiral anomaly) in systems with the Dirac spectrum of electrons, including superfluid ^{3}He-*A*, doped graphene, and topological superconductors.

DOI: 10.1134/S1063776114060132

CONTENTS

1. INTRODUCTION

Conduction electrons in metals and positive ions form a solid-state plasma that determines the complex of their electric, galvanomagnetic, kinetic, and superconducting properties. The coupling between the subsystems of massive positive ions and light fermions leads to the formation of electron–phonon interaction, which determines the properties of the electron subsystem. In particular, the effective interaction between electrons in the solid-state plasma can differ substantially from the Coulomb interaction of electrons in vacuum and can even change sign. This important effect forms the basis of the electron–phonon mechanism of the Cooper instability in traditional superconductors [1].

The role of mediator, interaction with which initiates the renormalization of the Coulomb interaction, can obviously be played by any other subsystem. It is necessary only that the interaction of the electron gas with such a subsystem leads to polarization effects resulting in the production of electrons and holes in the vicinity of the Fermi surface. In particular, in many theoretical publications on high-temperature superconductors, the role of such a mediator is played by collective excitations of the subsystem of localized spins of copper ions. This effect is associated with the spin-fluctuation mechanism of Cooper instability leading to the formation of a superconducting phase with *d*-wave type symmetry of the order parameter.

In the secondary quantization representation for fermions, the operator of Coulomb interaction between electrons contains nondiagonal terms initiat-

ing the polarization contributions to the groundstate energy in higher orders of perturbation theory. These contributions lead to renormalization of the Cooper interaction between electrons. Therefore, the effective interaction of electrons in such a substance can differ significantly from electron–electron interaction in vacuum. This makes topical the problem formulated for the first time by Anderson [2], associated with the possibility of renormalization of the Coulomb interaction between electrons, so that the effective electron–electron interaction becomes attractive and not repulsive even when phonons are disregarded. In other words, the problem involves searching for conditions in which the above-mentioned polarization effects in the electron plasma of solid metals reverse the sign of the resultant interaction between electrons. The analytic solution to this problem comes to calculating the effective pair interaction of electrons with allowance for many-particle effects in the electron ensemble. According to Anderson, an equally important problem is explaining the peculiar properties of the normal state of many strongly correlated electron systems above the superconducting transition temperature, especially in the pseudogap state.

Considerable advances have been made in recent decades in experimental and theoretical investigations of superconducting systems with a nonphonon origin of Cooper pairing. The first experimentally discovered systems with nontraditional triplet p-wave pairing (the total spin of a Cooper pair is $S_{\text{tot}} = 1$ and the orbital angular momentum is $l = 1$) were the superfluid A and B phases of ^{3}He with low superconducting transition temperatures $T_c \sim 1$ mK [3–5]. Other examples of systems in which p-wave pairing takes place are $^6Li_2$ and $^{40}K_2$ molecules in magnetic taps under Feshbach resonance conditions with ultralow superconducting transition temperatures $T_c \sim 10^{-7}$ to 10^{-6} K [6, 7]. It is assumed that nontraditional p-wave pairing with superconducting transition temperatures $T_c \sim 0.5$–1 K takes place in some heavy-fermion intermetallides such as $U_{1-x}Th_xBe_{13}$ and UNl_2Al_3 with high effective masses $m^* \sim (100–200)m_e$ [8, 9]. The p-wave paring is often mentioned in connection with organic superconductors such as α-(BEDT-TTF)$_2$I$_3$ with $T_c \sim 5$ K [10]. Finally, p-wave pairing with $T_c \sim 1$ K is apparently achieved in ruthenates Sr_2RuO_4 [11] and probably in layered dichalcogenides CuS_2–$CuSe_2$, semimetals, and semimetal superlattices InAs–GaSb and PbTe–SnTe. Nontraditional superconductors with singlet d-wave pairing ($S_{\text{tot}} = 0$, $l = 2$) include heavy-fermion intermetallide UPt_3 with $m^* \sim 200m_e$ and $T_c \sim 0.5$ K, as well as a wide class of high-T_c cuprate superconductors with superconducting transition temperatures from $T_c \sim 36$ K for lanthanum-based compounds to $T_c \sim 160$ K (the absolute record-highest value of T_c attained at present in cuprates) for mercury-based superconductors obtained under pressure. Finally, we should also mention (in connection with the nonphonon superconductivity problem) new multiband superconductors such as MgB_2 [12] and iron-arsenide-based superconductors with the more traditional s-wave pairing, which were discovered recently [13].

Apart from the problems of Cooper pairing in the above systems, the still unsolved problems associated with the search for superfluidity in 3D and, especially, 2D (thin films, submonolayers) solutions of ^{3}He in ^{4}He [3–5] and superconductivity in doped graphene [14] are of considerable interest. Such systems are the most promising for experimental and theoretical description of a wide class of physical phenomena, including nontraditional superconductivity.

In particular, ^{3}He submonolayers adsorbed on various substrates such as a solid substrate (grafoil) or the free surface of superfluid ^{4}He permit the various correlation regimes in the system (from ultrararefied Fermi gas to strongly correlated fermion system [15]) to be achieved with variation of the number density of particles in a wide range. This makes solutions ideal objects for the development and testing of various many-body methods in condensed matter theory.

Graphene is of considerable importance from the fundamental and applied viewpoints due to its unique electronic properties [16, 17]. In the vicinity of the Fermi level, electrons in graphene exhibit linear dispersion, and the energy gap between the valence band and the conduction band is absent. For this reason, electrons can be described by the 2D Dirac equation for zero-mass charged quasiparticles [18]. The properties of such quasiparticles (like reduced dimensionality, the spinor origin of the spectrum, zero mass, and the absence of a gap in the spectrum) lead to a number of nontrivial electronic effects that have no analogs in other physical systems [19].

Such systems stimulated an intense search for alternative superconducting pairing mechanisms, which are based on correlations in the Fermi liquid. The Kohn–Luttinger mechanism [20] proposed in 1965 is the most promising in this respect. This mechanism presumes the transformation of initial repulsive interaction of two particles in vacuum into effective attraction in the presence of the fermionic background. This review describes the main results on Kohn–Luttinger superconductivity in repulsive Fermi systems, which have been obtained in the last 50 years.

2. ELECTRON GAS MODEL

The Fermi gas model is the basic model for studying nonphonon superconductivity mechanisms in low-density electron systems. In the case of an attractive Fermi gas, the scattering length is negative ($a < 0$) and traditional s-wave pairing takes place (total spin $S = 0$ and orbital angular momentum $l = 0$) with the superconducting transition temperature

$$T_c^s \approx 0.28\varepsilon_F \exp\left(-\frac{\pi}{2|a|p_F}\right). \quad (1)$$

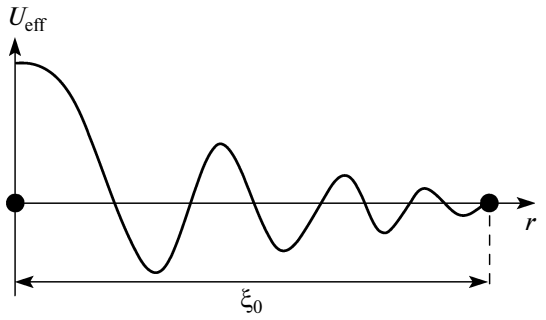

Fig. 1. Friedel oscillations in the effective interaction of two particles due to polarization of the fermionic background: ξ_0 is the coherence length of a Cooper pair; $\xi_0 \gg 1/p_F$.

This result was obtained in [21] soon after the formulation of the BCS theory [1]. Result (1) differs from the classical BCS formula. Namely, the quantity $0.28\varepsilon_F$ appears in the preexponential factor instead of the Debye frequency ω_D typical of models of traditional superconductors.

In the model of a repulsive Fermi gas, the scattering length is $a > 0$ and superconductivity in the low-temperature range emerges in accordance with the Kohn–Luttinger mechanism. The physical reason for this pairing mechanism is associated with the effective interaction of quasiparticles occurring as a result of polarization of the fermionic background. In fact, due to the sharp boundary existing in the momentum space, which is equal to the diameter $2p_F$ of the Fermi sphere and separates the region of filled states from the empty states, the effective interaction of quasiparticles at the Fermi level does not decrease exponentially, but has an alternating form (Friedel oscillations [22]); in the 3D case, we have

$$U_{\text{eff}}(r) \sim \frac{\cos(2p_F r)}{(2p_F r)^3}. \qquad (2)$$

If the distance between two electrons in a Cooper pair is much larger than the atomic spacing, effective interaction (2) in the coordinate space has a large number of maxima and minima (Fig. 1). Then the integrated effect determined by averaging of Friedel oscillations over such a potential relief can generally result in the effective attraction and the occurrence of superconductivity in the system.

Kohn and Luttinger [20], who investigated a 3D electron gas, were the first to pay attention to this superconductivity mechanism. They showed that the effective interaction in the first two orders of perturbation theory can be described by the sum of five diagrams shown in Fig. 2. The first diagram corresponds to the initial interaction of two electrons in the Cooper channel. The next four (Kohn–Luttinger) diagrams reflect second-order processes and take into account the polarization effects in the filled Fermi sphere. In the case of a low-density Fermi gas and a short-range potential, the contribution to the effective interaction is determined only by the fourth (exchange) diagram; in the first two orders of perturbation theory in gas parameter ap_F, the expression for U_{eff} can be written in the form

$$U_{\text{eff}}(\mathbf{p}, \mathbf{k}) = ap_F + (ap_F)^2 \Pi(\mathbf{p} + \mathbf{k}), \qquad (3)$$

where $\Pi(\mathbf{p} + \mathbf{k})$ is the static polarization operator described by the standard Lindhard function [23, 24]

$$\Pi(\mathbf{p} + \mathbf{k}) = \frac{1}{N}\sum_{\mathbf{p}_1} \frac{n_F(\varepsilon_{\mathbf{p}_1 - \mathbf{p} - \mathbf{k}}) - n_F(\varepsilon_{\mathbf{p}_1})}{\varepsilon_{\mathbf{p}_1} - \varepsilon_{\mathbf{p}_1 - \mathbf{p} - \mathbf{k}}}, \qquad (4)$$

which is responsible for charge screening in the case of the electron gas in a metal. Here, $\varepsilon_{\mathbf{p}} = \mathbf{p}^2/2m$ is the energy spectrum,

$$n_F(x) = \left(\exp\left(\frac{\varepsilon - \mu}{T}\right) + 1\right)^{-1}$$

is the Fermi–Dirac distribution function, and μ is the chemical potential.

It was noted in early publications by Migdal [25] and Kohn [26], as well as in [20], that at low temperatures ($T \ll \varepsilon_F$), the polarization operator contains, in addition to the regular part, a singular part also, which is known as the Kohn singularity and has the following form in the 3D space:

$$\Pi_{\text{sing}}(\tilde{q}) \sim (\tilde{q} - 2p_F)\ln|\tilde{q} - 2p_F|, \qquad (5)$$

where $\tilde{q} = |\mathbf{p} + \mathbf{k}|$ for the fourth exchange diagram in Fig. 2. As we pass to the coordinate space, singular part Π_{sing} leads to Friedel oscillations (2) in the effective interaction (see Fig. 1). Thus, the purely repulsive short-range potential acting between two particles in vacuum induces the effective interaction in the electron gas with the competition between repulsion and attraction. It turns out that the singular part in U_{eff}

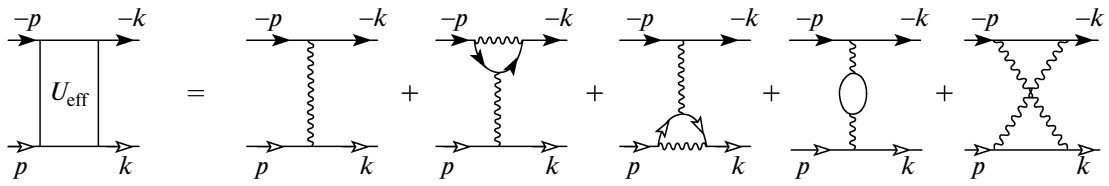

Fig. 2. First- and second-order diagrams for effective interaction U_{eff}. Solid lines with light (dark) arrows correspond to the electron Green's function with a spin projection of +1/2 (−1/2). Wavy lines reflect the initial interaction.

operates in favor of attraction, ensuring a contribution that always exceeds the repulsive contribution associated with the regular part of U_{eff} for the orbital angular momenta $l \neq 0$ of a pair. This leads to superconducting instability with the critical temperature $T_{\text{cl}} \sim \exp(-l^4)$ for large orbital angular momenta $l \gg 1$. In this case, conventional pairing in the s-wave channel ($l = 0$) is suppressed by purely Coulomb repulsion associated with the main maximum in U_{eff} (see Fig. 1), and superconductivity is observed for large values of orbital angular momentum $l \gg 1$. It should be noted that for $l \neq 0$, the role of the main maximum is suppressed by the centrifugal potential, which improves the conditions for the occurrence of superconductivity.

Thus, publication [20] led to the nontrivial conclusion that Fermi systems do not exist in the normal state at zero temperature because any 3D electron system with the initial repulsive interaction between particles at very low temperatures is unstable to the transition to the superconducting state with a large orbital angular momentum ($l \gg 1$) of the relative motion of a Cooper pair. However, the estimates for the superconducting transition temperature obtained in [20] for the realistic parameters of electron systems in a metal and for superfluid ^{3}He gave very low values of the superconducting transition temperature ($T_{\text{cd}} \sim 10^{-16}$ K for ^{3}He and $T_{\text{cd}} \sim 10^{-11}$ K for the metal plasma for the value of $l = 2$ considered in [20]). Such a low T_c value was one of the reasons the Kohn–Luttinger mechanism was overlooked by researchers for a long time.

It was shown in later publications [27, 28] that the superconducting transition temperature was underestimated in [20] because the asymptotic expression for large orbital angular momenta $l \gg 1$ was used. Indeed, for $l = 1$, exact analytic calculations show that the contributions to U_{eff} corresponding to attraction of quasiparticles again prevail over the repulsive contributions. As a result, a 3D repulsive Fermi gas turns out to be unstable to the superconducting transition with triplet p-wave pairing at the superconducting transition temperature [27–30], which is determined by the principal exponential:

$$T_{\text{cp}} \approx \varepsilon_F \exp\left(-\frac{5\pi^2}{4(2\ln 2 - 1)(ap_F)^2}\right) = \varepsilon_F \exp\left(-\frac{13}{\lambda^2}\right), \quad (6)$$

where $\lambda = 2ap_F/\pi$ is the effective 3D Galitskii gas parameter [31]. It should be noted that for $l = 1$, the contribution of the Kohn singularity only increases T_{cp}, but does not play a decisive role in the occurrence of superconductivity.

It was shown in [32] that the superconducting transition temperature can appreciably be elevated even for low electron densities by placing a system of neutral particles into a magnetic field. This is due to the fact that in contrast to s-wave pairing, paramagnetic suppression of superconductivity does not take place in the p-wave channel and the value of T_{cp} may increase due to the enhancement of the effective interaction and due to the specific form of the Kohn singularity. In this case, the critical temperature T_{cp} correspond to the so-called A_1 phase, in which a Cooper pair is formed by two "up" spins, while the effective interaction for them is prepared by two "down" spins.

In the case of a low-density 2D repulsive Fermi gas, the effective interaction in the first two orders of perturbation theory in the gas parameter has the form [33, 34]

$$U_{\text{eff}}(\mathbf{p}, \mathbf{k}) = f_0 + f_0^2 \Pi(\mathbf{p} + \mathbf{k}), \quad (7)$$

where $f_0 = 1/2\ln(p_F r_0)$ is the 2D Bloom gas parameter [35], $\Pi(\mathbf{p} + \mathbf{k})$ is the 2D polarization operator, and r_0 is the range of the potential.

In the 2D situation, the effective interaction in the coordinate space also contains Friedel oscillations

$$U_{\text{eff}}(r) \sim f_0^2 \frac{\cos(2p_F r)}{(2p_F r)^2}, \quad (8)$$

which are much stronger than oscillations (2) in the 3D case. However, the 2D Kohn singularity in the momentum space has one-sided character [36]:

$$\Pi_{\text{sing}}(\tilde{q}) \sim f_0^2 \operatorname{Re}\sqrt{\tilde{q} - 2p_F} = 0 \quad (9)$$

for $\tilde{q} = (\mathbf{p} + \mathbf{k}) \leq 2p_F$ and is ineffective for the problem of superconductivity. Thus, a 2D repulsive Fermi gas remains in the normal state at least in the first two orders of perturbation theory in gas parameter f_0. Nevertheless, it was shown in [33] that superconducting p-wave pairing appears in the next (third) order of perturbation theory in f_0, in which the singular contribution to the effective interaction has the form

$$\Pi_{\text{sing}}(\tilde{q}) \sim f_0^3 \operatorname{Re}\sqrt{2p_F - \tilde{q}}. \quad (10)$$

Exact calculations [37] of the superconducting transition temperature taking into account all irreducible third-order diagrams leads to the expression

$$T_{\text{cp}} \sim \varepsilon_F \left(-\frac{1}{6.1 f_0^3}\right). \quad (11)$$

In this case, the superconducting transition temperature is estimated as 10^{-4} K [33, 37] for the limiting densities for which the Fermi-gas description is still applicable. This estimate is closer to the realistic values predicted for ^{3}He monolayers on the ^{4}He surface [38].

Another possibility to sharply increase T_c at low density is associated with the analysis of the two-band situation or a multilayer system. In this case, the role of "up" spins is played by electrons from the first band (layer), while the role of "down" spins is played by electrons of the second band (layer). The coupling between electrons of the two bands is accomplished via interband Coulomb interaction. As a result, the following mechanism of superconducting pairing is possible: electrons of one species form a Cooper pair by

polarizing electrons of the other species [39, 40]. This mechanism of interaction is also effective in quasi-two-dimensional systems.

It should be noted that some authors [41, 42] also studied the effect of split-off energy bands on the properties of the normal state in the basic models for repulsive Fermi systems. For example, nontrivial corrections to the Galitskii–Bloom Fermi-gas expansion appear due to antibound states [41] in the 2D Hubbard model or due to a singularity in the Landau quasiparticle f-function in a repulsive 2D Fermi gas at low electron density [42]. It was shown in [41, 42], however, that these corrections do not destroy the Landau Fermi-liquid picture in the 3D or in the 2D case.

3. HUBBARD MODEL

The Hubbard model [44], which is one of fundamental models for describing peculiar properties of cuprates, has become very popular in connection with the discovery of high-temperature superconductivity [43]. The Hubbard model is a special case of a more general model of interacting electrons whose band structure can be described using the tight-binding method; in fact, the Hubbard model is the minimal model taking into account the band motion of electrons in a solid along with strong electron–electron interaction [45–49]. This model is especially important for describing narrow-band metals [37]. In the secondary quantization representation, the Hamiltonian of such a model can be written in the form

$$\hat{H} = \sum_{f\sigma}(\varepsilon - \mu)n_{f\sigma} + \sum_{fm\sigma} t_{fm} c^{\dagger}_{f\sigma} c_{m\sigma} + U\sum_{f} n_{f\uparrow} n_{f\downarrow}, \tag{12}$$

where $c^{\dagger}_{f\sigma}$ ($c_{f\sigma}$) is the creation (annihilation) operator for an electron with spin projection $\sigma = \pm 1/2$ at the f site, ε is the single-site electron energy, and μ is the chemical potential of the system. In expression (12),

$$n_f = \sum_{\sigma} n_{f\sigma} = \sum_{\sigma} c^{\dagger}_{f\sigma} c_{f\sigma}$$

is the operator of the particles density at site f, matrix element t_{fm} determines the intensity of electron hoppings from site f to site m, and U is the Coulomb interaction parameter for two electrons located at the same site and having opposite projections of the spin moment (Hubbard repulsion).

Since a large body of experimental data indicated that the main dynamics of Fermi excitations in cuprates evolves in the CuO_2 planes, the 2D Hubbard model on a simple square lattice was mainly used to describe the nonphonon mechanisms of high-temperature superconductivity. In the momentum space, the Hamiltonian of the Hubbard model has the form

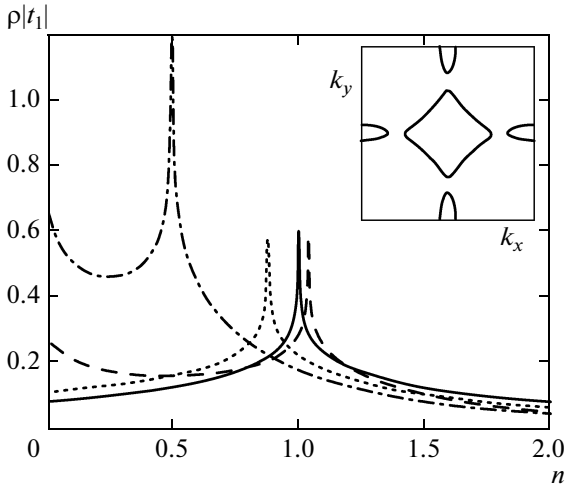

Fig. 3. Modification of the electron density of states and the shift of the Van Hove singularity in the Hubbard model on a square lattice upon a change in the hopping integral: $t_2 = t_3 = 0$ (solid curve), $t_2 = 0.15$, $t_3 = 0$ (dotted curve), $t_2 = 0.15$, $t_3 = 0.1$ (dashed curve), and $t_2 = 0.44$, $t_3 = 0$ (dot-and-dash curve). The inset shows the formation of a multisheet Fermi contour for the set of parameters $t_2 = 0.44$, $t_3 = -0.1$, and $\mu = 2$ (all parameters are given in units of $|t_1|$).

$$\hat{H} = \sum_{\mathbf{p}\sigma}(\varepsilon_{\mathbf{p}} - \mu)c^{\dagger}_{\mathbf{p}\sigma} c_{\mathbf{p}\sigma} + U\sum_{\mathbf{pp'q}} c^{\dagger}_{\mathbf{p}\uparrow} c^{\dagger}_{\mathbf{p'}+\mathbf{q}\downarrow} c_{\mathbf{p}+\mathbf{q}\downarrow} c_{\mathbf{p'}\uparrow}, \tag{13}$$

where the electron energy taking into account distant hoppings, whose intensity is determined by parameters t_2 and t_3, is described by the expression

$$\varepsilon_{\mathbf{p}} = 2t_1(\cos p_x d + \cos p_y d) + 4t_2 \cos p_x d \cos p_y d + 2t_3(\cos 2p_x d + \cos 2p_y d), \tag{14}$$

where d is the intersite distance. It should be noted that in simulating electron spectrum (14) and constructing the phase diagram of the superconducting state in the Hubbard model, it becomes important to exceed the bounds of the nearest-neighbor approximation ($t_2 \neq 0$, $t_3 \neq 0$). This is due to the fact that the main contribution to the effective coupling constant comes from the interaction of electrons on the Fermi surface with a geometry depending on the structure of the energy spectrum. The fact that the inclusion of distant hoppings shifts the Van Hove singularity in the density of electron states from half-filling ($n = 1$) to the regions of lower or higher electron densities (Fig. 3) also plays an important role. It should be noted that the inclusion of hoppings to the third coordination sphere of the square lattice ($t_3 \neq 0$) can lead to a qualitative change in the Fermi surface geometry

(in particular, to the formation of a multisheet Fermi contour; see the inset to Fig. 3).

Thus, the allowance for distant hoppings can modify the phase diagram determining the range of superconducting states with various types of the order parameter symmetry.

In the Hubbard model, perturbation theory can be constructed in two limiting cases, viz., the Born approximation with a shallow potential well ($U \ll W$, where $W = 2zt$ is the bandwidth and z is the number of the nearest neighbors) and an arbitrary electron density, and in the case of strong coupling ($U \gg W$) and a low electron density. The application of the weak coupling approximation ($U \ll W$) for analyzing the possibility of Kohn–Luttinger pairing makes it possible to calculate U_{eff} for the Cooper channel in the electron density range $n \sim 1$ (in the vicinity of half-filling) using diagrams of no higher than the second order in the interaction (see Fig. 2). In the opposite limit of strong coupling ($U \gg W$), the use of diagrams of only the first and second orders is valid only for a low electron density $n \ll 1$, for which the Galitskii–Bloom Fermi gas expansion is valid [31, 35].

In [50], the authors analyzed the conditions of the Kohn–Luttinger superconductivity realization in the 2D Hubbard model with Hamiltonian (13) in the weak-coupling limit ($U \ll W$) in the nearest neighbor approximation ($t_2 = t_3 = 0$) at the low electron densities ($p_F d \ll 1$):

$$\varepsilon_{\mathbf{p}} - \mu = 2t_1(\cos p_x d + \cos p_y d) - \mu \approx \frac{p^2 - p_F^2}{2m} - \frac{(p_x^4 + p_y^4)d^2}{24m} + \frac{(p_x^6 + p_y^6)d^4}{720m}, \quad (15)$$

where $m = 1/(2t_1 d^2)$ is the band mass of an electron. It can be seen that the initial electron spectrum in the chosen approximation for $p_F d \ll 1$ almost coincides with the spectrum of a noninteracting Fermi gas, and the Hubbard Hamiltonian itself is identically equivalent to the Hamiltonian of a weakly nonideal Fermi gas with a short-range repulsion between particles. To verify the possibility of a superconducting transition in this approximation, the effective initial vertex for the Cooper channel was calculated up to the second order of perturbation theory inclusively:

$$U_{\text{eff}}(\mathbf{p}, \mathbf{k}) = U + U^2\Pi(\mathbf{p} + \mathbf{k}), \quad (16)$$

where $\Pi(\mathbf{p} + \mathbf{k})$ is polarization operator (4).

To solve the Bethe–Saltpeter integral equation, in [50] the eigenfunctions of the irreducible representations of symmetry group C_{4v} of the square lattice have been used. This group is known to have five irreducible representations [51], for each of which the integral equation has its own solution. Among these representations, there are four 1D representations A_1, A_2, B_1, and B_2, which correspond to singlet pairing, as well as a 2D representation E corresponding to triplet pairing. The explicit form of orthonormal functions $g_m^{(\alpha)}(\phi)$ (superscript "α" denotes an irreducible representation, m is the number of the basis function of the representation α, and ϕ is the angle characterizing the direction of the momentum $\hat{\mathbf{p}}$ lying on the Fermi contour relative to the p_x axis) and the symmetry classification of superconducting order parameter $\Delta^{(\alpha)}(\phi)$ are defined as

$$\begin{aligned}
A_1 &\longrightarrow g_m^{(s)}(\phi) = \frac{1}{\sqrt{(1+\delta_{m0})\pi}}\cos 4m\phi, \\
&m \in [0, \infty), \\
A_2 &\longrightarrow g_m^{(s_{\text{ext}})}(\phi) = \frac{1}{\sqrt{\pi}}\sin 4(m+1)\phi, \\
B_1 &\longrightarrow g_m^{(d_{xy})}(\phi) = \frac{1}{\sqrt{\pi}}\sin(4m+2)\phi, \\
B_2 &\longrightarrow g_m^{(d_{x^2-y^2})}(\phi) = \frac{1}{\sqrt{\pi}}\cos(4m+2)\phi, \\
E &\longrightarrow g_m^{(p)}(\phi) = \frac{1}{\sqrt{\pi}}(A\sin(2m+1)\phi \\
&\quad + B\cos(2m+1)\phi).
\end{aligned} \quad (17)$$

To solve the problem of superconducting pairing, function $U_{\text{eff}}(\mathbf{p}, \mathbf{k})$ was expanded into a series with functions (17), after that the sign of expressions for U_{eff}^{α} was analyzed. As a result, it was shown that the 2D electron system described by the Hubbard model for a small occupancy and for $U \ll W$ is unstable to the pairing with the d_{xy}-wave type of symmetry of the order parameter $\Delta(\phi)$.

The weak-coupling limit ($U < W$) in the 3D and 2D Hubbard models in the vicinity of half-filling was analyzed in [52, 53]. In the 2D case [53], for $n \approx 1$ in the nearest neighbor approximation, the electron spectrum becomes quasi-hyperbolic [56],

$$\varepsilon_{\mathbf{p}} \approx \pm\frac{p_x^2 - p_y^2}{2m}, \quad (18)$$

for small values of $p_x d < 1$ and $p_y d < 1$ in the vicinity of corner points $(0, \pm\pi)$ and $(\pm\pi, 0)$, at which the Fermi surface almost touches the Brillouin zone (Fig. 4). In expression (18), the band mass is $m = 1/(2t_1 d^2)$ as before. It is well known that the density of electron states in these regions near the Van Hove singularity is logarithmically large ($g(E) \sim \ln(t/|\mu|)$, where $\mu \ll t$ is the chemical potential in the vicinity of half-filling). It can be seen from Fig. 4 that there are two almost planar regions near the Fermi surface, which satisfy the ideal nesting condition for the exactly half-filled state ($n = 1$):

$$\varepsilon_{\mathbf{p}+\mathbf{Q}} = -\varepsilon_{\mathbf{p}}, \quad (19)$$

where $\mathbf{Q} = (\pi/d, \pi/d)$ is the nesting vector for a 2D square lattice. In these regions, the polarization operator is enhanced by the Kohn singularity, as well as by the Van Hove singularity, and has the form [53, 56]

$\Pi(\mathbf{Q}) \sim \ln^2(t/|\mu|)$. In this case, the parameter of perturbation theory is the quantity

$$f_0 = \frac{U}{8\pi t} \ll 1, \tag{20}$$

and the expression for the effective interaction in the second order of perturbation theory in f_0 has the form [53]

$$U_{\text{eff}} \sim f_0 + f_0^2 \ln^2 \frac{t}{|\mu|}. \tag{21}$$

Since the expression for the Cooper loop for $n \approx 1$ contains, apart from the conventional Cooper logarithm, the logarithm of the Van Hove singularity as well, we can ultimately write

$$L(\xi_{\mathbf{p}}) = \frac{1}{N}\sum_{\mathbf{p}} \frac{\tanh(\xi_{\mathbf{p}}/2T)}{2\xi_{\mathbf{p}}} \sim \ln\frac{\mu}{T}\ln\frac{t}{|\mu|}, \tag{22}$$

where $\xi_{\mathbf{p}} = \varepsilon_{\mathbf{p}} - \mu$. Therefore, the equation for the temperature of the superconducting transition to the phase with the $d_{x^2-y^2}$-wave symmetry of the order parameter derived in [53] in the main logarithmic approximation has the form

$$f_0^2 \ln^3 \frac{t}{|\mu|} \ln\frac{\mu}{T_c} \sim 1. \tag{23}$$

Hence, the superconducting transition temperature is given by

$$T_c^{d_{x^2-y^2}} \sim \mu \exp\left(-\frac{1}{f_0^2 \ln^3(t/|\mu|)}\right). \tag{24}$$

This expression shows that the small value of f_0^2 for $f_0 \ll 1$ is compensated by the large value of $\ln^3(t/|\mu|) \gg 1$.

The results obtained in [50] on d_{xy}-wave pairing for $n \lesssim 0.6$ and $d_{x^2-y^2}$-wave pairing for $n \sim 1$ [52, 23] in the strong coupling limit were subsequently confirmed by other authors too. In [54], the phase diagram of the superconducting state was constructed in the 2D Hubbard model at low and intermediate electron densities; this diagram reflected the dependence of the competition of various symmetry types of the order parameter on integral t_2 of electron hopping to the next-to-nearest neighbors sites. The phase diagram obtained in the second order of perturbation theory shows that for $t_2 = 0$, in the range of low electron densities $0 < n < 0.52$, superconductivity with the d_{xy}-wave type of the order parameter symmetry is realized in the first two orders of perturbation theory; in the interval $0.52 < n < 0.58$, the ground state corresponds to a phase with p-wave pairing, while for $n > 0.58$, $d_{x^2-y^2}$-wave pairing appears. Analogous results were obtained in [55] using the renormalized group method.

In the immediate vicinity of the half-filling ($0.95 < n < 1$), where strong competition between superconductivity and antiferromagnetism takes place, the problem of the Cooper instability was considered in [56, 57]. In these publications, the so-called parquet diagrams were summed up and the following relation was obtained for $\mu \sim T_c$:

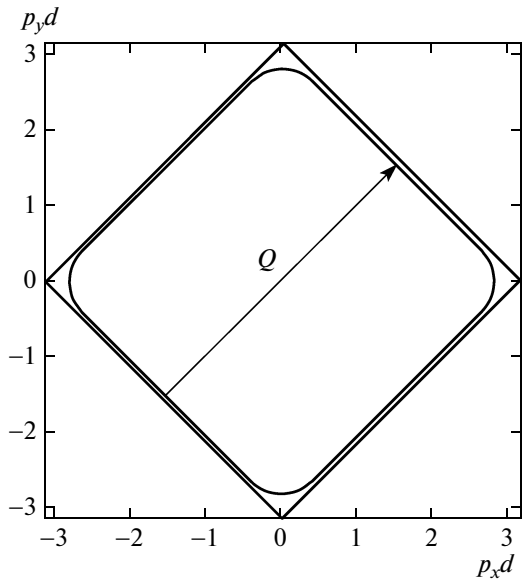

Fig. 4. Fermi surface in the case of a nearly half-filled band ($n \approx 1$) in the 2D Hubbard model on a square lattice, where $\mathbf{Q} = (\pi/d, \pi/d)$ is the nesting vector.

$$f_0^2 \ln^4 \frac{t}{|\mu|} \sim f_0^2 \ln^4 \frac{t}{T_c} \sim 1. \tag{25}$$

This relation leads to an elegant estimate of the maximal superconducting transition temperature:

$$T_c^{d_{x^2-y^2}} \sim t \exp\left(-\frac{\text{const}}{\sqrt{f_0}}\right). \tag{26}$$

It should be noted that the maximal superconducting transition temperature in the 2D Hubbard model was also obtained in [58] in the regime $U/W \sim 1$ for optimal electron concentrations $n \sim 0.8$–0.9. According to the estimate obtained in [58], the superconducting transition temperature at the maximum can reach desirable values $T_c^{d_{x^2-y^2}} \approx 100$ K, which are realistic for optimally doped cuprate superconductors.

4. SHUBIN–VONSOVSKY MODEL

The important question concerning the role of full Coulomb interaction in nonphonon superconductivity mechanisms, which in fact includes not only short-range Hubbard repulsion, but also the long-range component, was considered in [59]. The authors of [59] considered the 3D jelly model for realistic values of electron densities with $r_S \leq 20$, where

$$r_S = 1.92/p_F a_B \tag{27}$$

is the Wigner–Seitz correlation radius and $a_B = \varepsilon_0/me^2$ is the Bohr radius of electron ($\hbar = 1$). In calculation of the effective interaction, the contributions of the first and second orders of perturbation theory associated with all diagrams in Fig. 2 were taken into account. It was noted in [59] that previous investigations of Kohn–Luttinger superconductivity were limited to the inclusion of only short-range Coulomb interaction U of electrons in view of computational difficulties associated with taking into account the Fourier transform of the long-range Coulomb repulsion $V_{\mathbf{q}}$, which depends on $\mathbf{q}$ in the first- and second-order diagrams. As a result, the strong initial Coulomb repulsion in the first order of perturbation theory (first diagram in Fig. 2) was disregarded, and the contribution to the effective interaction of electrons in the Cooper channel was due only to the last exchange diagram in Fig. 2. This contribution was attractive by nature and ensured p-wave pairing in the 3D case [27, 28] and the d-wave pairing in the 2D case [29, 58] in the Hubbard model.

In [59], the long-range Coulomb interaction $V_{\mathbf{q}}$ was chosen in the form of the Fourier transform of the Yukawa potential

$$V(r) = \frac{e^2}{r}\exp(-\kappa r),$$

$V_{\mathbf{q}}$ has the following standard form in the 3D case:

$$V_{\mathbf{q}} = \frac{4\pi e^2}{q^2 + \kappa^2}, \tag{28}$$

where κ is the inverse screening length. It was concluded in [59] from the results of calculations that small and intermediate values of Hubbard repulsion U in the presence of the long-range part of Coulomb interaction (28) do not induce realization of the Cooper instability in 3D and 2D Fermi systems in the p-wave and d-wave channels, irrespective of the value of the small screening length. The pairing that occurs for large orbital angular momenta ($l \geq 3$) leads to almost zero values of the superconducting transition temperature for any realistic value of the Fermi energy. Thus, anomalous pairing associated with strong Coulomb repulsion is impossible according to the authors of [59], because the corresponding energy of condensation for Cooper pairs is several times lower than the energy of condensation associated with electron–phonon interaction.

The rising interest in the role of the long-range intersite Coulomb correlations in the structure of the phase diagram of high-T_c superconductors has made the extended Hubbard model popular. This model takes into account not only one-site Hubbard repulsion, but the interaction of electrons at different sites of the crystal lattice (in the Russian literature, this model is usually referred to as the Shubin–Vonsovsky model [60]).

Historically, this model was formulated almost immediately after the origination of quantum mechanics and is a predecessor of some important models in condensed matter theory (in particular, the s–$d(f)$ model and the Hubbard model). The Shubin–Vonsovsky model was actively used in analyzing polaron states in solids [61] and the metal–insulator transition [62], as well as in studying the effect of the intersite Coulomb interaction on the superconducting properties of strongly correlated systems [63–65].

In the Wannier representation, the Hamiltonian of the Shubin–Vonsovsky model can be written in the form

$$\hat{H} = \sum_{f\sigma}(\varepsilon - \mu)c^\dagger_{f\sigma}c_{f\sigma} + \sum_{fm\sigma} t_{fm}c^\dagger_{f\sigma}c_{m\sigma} + U\sum_f \hat{n}_{f\uparrow}\hat{n}_{f\downarrow} + \frac{1}{2}\sum_{fm} V_{fm}\hat{n}_f\hat{n}_m, \tag{29}$$

where the last term corresponds to the allowance for energy V_{fm} of the Coulomb interaction of electrons from different sites of the crystal lattice and $\hat{n}_f$ is the total density operator. The last three terms in Hamiltonian (29) together reflect the fact that the screening radius in the systems under investigation may be by several times larger than the unit cell parameter [62]. This ensures an advantage of the Shubin–Vonsovsky model, in which the intersite Coulomb interaction is taken into account within several coordination spheres. In the momentum representation, Hamiltonian (29) assumes the form

$$\hat{H} = \sum_{\mathbf{p}\sigma}(\varepsilon_{\mathbf{p}} - \mu)c^\dagger_{\mathbf{p}\sigma}c_{\mathbf{p}\sigma} + U\sum_{\mathbf{pp'q}} c^\dagger_{\mathbf{p}\uparrow}c^\dagger_{\mathbf{p'}+\mathbf{q}\downarrow}c_{\mathbf{p}+\mathbf{q}\downarrow}c_{\mathbf{p'}\uparrow} + \frac{1}{2}\sum_{\mathbf{pp'q}\sigma\sigma'} V_{\mathbf{p}-\mathbf{p'}}c^\dagger_{\mathbf{p}\sigma}c^\dagger_{\mathbf{p'}+\mathbf{q}\sigma'}c_{\mathbf{p}+\mathbf{q}\sigma'}c_{\mathbf{p'}\sigma}, \tag{30}$$

where the Fourier transform of the Coulomb interaction of electrons at the nearest sites (V_1) and at the next-to-nearest sites (V_2) in the 2D case on the square lattice has the form

$$V_{\mathbf{q}} = 2V_1(\cos q_x d + \cos q_y d) + 4V_2\cos q_x d\cos q_y d. \tag{31}$$

The authors of [66] contributed to the discussion [58, 59] by analyzing the conditions for the occurrence of superconducting Kohn–Luttinger pairing in the 3D and 2D Shubin–Vonsovsky models with Coulomb repulsion of electrons at neighboring sites ($V_1 \neq 0$, $V_2 = 0$). Instead of Yukawa potential (28) used as the Fourier transform of the intersite interaction, the situation of extremely strong Coulomb repulsion ($U \gg V_1 \gg W$) was considered. In the low electron density limit ($p_F d \ll 1$), it was shown that even in this most unfavorable case for the occurrence of effective attraction and superconductivity, the contribution from intersite Coulomb repulsion V_1 to the effective interaction in the p-wave channel is proportional to $(p_F d)^3$ in the 3D case and to $(p_F d)^2$ in the 2D case in accordance with the general quantum-mechanical results for slow particles in vacuum [51]. However,

these repulsive contributions cannot compensate contributions favoring attraction and proportional to $(p_F d)^2$ in the 3D case and to $1/\ln^3[1/(p_F d)^2]$ in the 2D case. It should be noted in this connection that the effective attraction appears only if the fermionic background is filled.

Thus, the previous results on Kohn–Luttinger superconducting p-wave pairing being attained both in the 2D and 3D Hubbard model with repulsion in the strong coupling limit ($U \gg W$) at low electron density hold even when strong Coulomb repulsion of electrons at neighboring sites ($V_1 \gg W$) is included in the Shubin–Vonsovsky model. As a result, the same expressions (6) and (11) for the temperature of the superconducting transition to the phase with p-wave type symmetry, like in the absence of interstitial Coulomb repulsion ($V_1 = 0$), are obtained in the 3D and 2D cases. Allowance for V_1 changes only the preexponential factor [37]; therefore, superconducting p-wave pairing can be realized in Fermi systems with purely Coulomb repulsion [66] in the absence of electron–phonon interaction.

A similar analysis was carried out in [67] for the extended Hubbard model in the Born weak coupling approximation, and the results were the same as in [66]. Moreover, it was noted in [67] that even in the weak coupling regime ($W > U > V$), in which controllable calculations can be performed, the effect of long-range Coulomb interactions is suppressed in view of the deterioration of the conditions for the evolution of the Cooper instability. As a matter of fact, long-range interactions in the lattice models usually contribute only to certain pairing channels and do not affect other channels. At the same time, the polarization contributions described by the diagrams in Fig. 2 have components in all channels, and more than one such component usually favors attraction. In such a situation, long-range interactions probably either do not affect at all the main component of the effective interaction leading to pairing, or they suppress the principal components without influencing secondary ones.

In this connection, a phase diagram was constructed in [67] on using the extended Hubbard model with the Kohn–Luttinger mechanism; this diagram visually reflected the result of competition of superconducting phases with different types of order parameter symmetry. The effective coupling constant was calculated using the following expression for the renormalized scattering amplitude in the Cooper channel:

$$U_{\text{eff}}(\mathbf{p}, \mathbf{q}) = U + V_{\mathbf{p}-\mathbf{q}} + U^2\Pi(\mathbf{p}+\mathbf{q}), \qquad (32)$$

where $V_{\mathbf{p}-\mathbf{q}}$ is the Fourier transform of the interstitial Coulomb repulsion (31) and $\Pi(\mathbf{p}+\mathbf{q})$ is Lindhard function (4). Thus, the interstitial Coulomb interaction V in [67] was taken into account only in the first order of perturbation theory, and the polarization contributions were determined only by the terms of the order U^2. It was shown [67] that long-range interaction has a tendency to suppress anomalous pairing in some channels; in spite of this the Kohn–Luttinger superconductivity survives in the entire range of electron concentrations $0 < n < 1$ and for all relations between the model parameters.

It was noted in [68] that effective interaction $U_{\text{eff}}(\mathbf{q})$ is characterized by a quadratic dependence on quasimomentum only in the range of $\mathbf{qd} \ll 1$. Beyond this range, it is important that the momentum dependence of $V_{\mathbf{q}}$ is determined by periodic functions. As a result, the behavior of $U_{\text{eff}}(\mathbf{q})$ is substantially modified as compared to the momentum dependence of the Fourier transform of the Yukawa potential. These factors considerably affect the conditions for the Cooper instability for large electron density values, when the Fermi surface does not exhibit spherical symmetry. Therefore, it should be expected that the conditions for superconducting pairing according to the Kohn–Luttinger mechanism are determined not only by dynamic effects associated with Coulomb interactions, but also by Brillouin zone effects.

The effect of the Coulomb interaction of electrons from the first and second coordination spheres on the realization of the Cooper instability was taken into account in [68] using the Shubin–Vonsovsky model in the Born weak coupling approximation ($W > U > V$). Accordingly, in the calculating the scattering amplitude in the Cooper channel, effective interaction $U_{\text{eff}}(\mathbf{p}, \mathbf{k})$ determined in graph form by the sum of the five diagrams (see Fig. 2) was used as the effective interaction of two electrons with opposite values of momentum and spin. The analytic form of this interaction is

$$U_{\text{eff}}(\mathbf{p}, \mathbf{k}) = U + V_{\mathbf{p}-\mathbf{k}} + \delta U(\mathbf{p}, \mathbf{k}), \qquad (33)$$

where the second-order corrections are given by

$$\begin{aligned}\delta U(\mathbf{p}, \mathbf{k}) = {} & \frac{1}{N}\sum_{\mathbf{p}_1}(U + V_{\mathbf{p}-\mathbf{k}}) \\ & \times (2V_{\mathbf{p}-\mathbf{k}} - V_{\mathbf{p}_1+\mathbf{p}} - V_{\mathbf{p}_1-\mathbf{k}}) \\ & \times \frac{n_F(\varepsilon_{\mathbf{p}_1}) - n_F(\varepsilon_{\mathbf{p}_1+\mathbf{p}-\mathbf{k}})}{\varepsilon_{\mathbf{p}_1} - \varepsilon_{\mathbf{p}_1+\mathbf{p}-\mathbf{k}}} \\ & + \frac{1}{N}\sum_{\mathbf{p}_1}(U + V_{\mathbf{p}_1-\mathbf{p}})(U + V_{\mathbf{p}_1-\mathbf{k}}) \\ & \frac{n_F(\varepsilon_{\mathbf{p}_1}) - n_F(\varepsilon_{\mathbf{p}_1-\mathbf{p}-\mathbf{k}})}{\varepsilon_{\mathbf{p}_1-\mathbf{p}-\mathbf{k}} - \varepsilon_{\mathbf{p}_1}}.\end{aligned} \qquad (34)$$

If the intersite Coulomb interaction is taken into account only in the first order and only for electrons at the nearest sites ($V_1 \neq 0$ and $V_2 = 0$ in formula (31)), and the excitation spectrum is described by only one hopping parameter ($t_1 \neq 0$, $t_2 = t_3 = 0$), the phase diagram of superconducting states for $U = |t_1|$ contains five regions (Fig. 5). In constructing this diagram, we used expression (32) for the effective interaction of

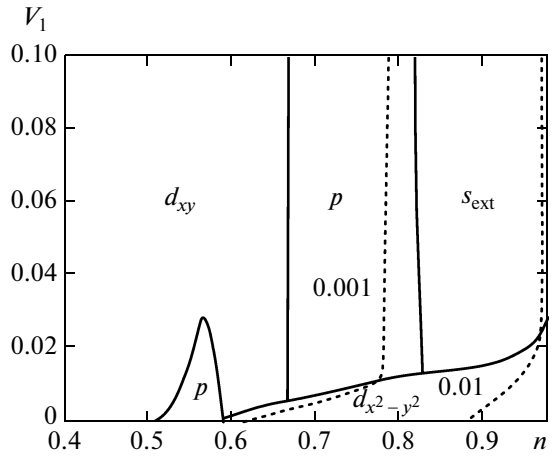

Fig. 5. Phase diagram in the Shubin–Vonsovsky model for $t_2 = t_3 = 0$, $U = |t_1|$ and $V_2/V_1 = 0$. The intersite Coulomb interaction is taken into account only in the first order of perturbation theory. For all points belonging to the same dotted curve, the value of λ is constant and marked by the corresponding numeral.

electrons in the Cooper channel; in this expression, the contributions proportional to UV and V^2 and appearing in expression (34) are disregarded. The segments of the phase diagram lying on the abscissa axis ($V_1 = 0$) agree with the regions on the phase diagram obtained in [54] for the Hubbard model.

Since the first order of perturbations theory in the intersite Coulomb interaction always has a tendency to suppress the superconducting pairing, the possibility of the Cooper instability realization based on the Kohn–Luttinger mechanism is associated with the occurrence (in the second order of perturbation theory) of contributions to the effective interaction matrix for the Cooper channel (34), which correspond to attraction and are quite intense. Thus, when the Kohn–Luttinger effects in the intersite Coulomb interaction are taken into account, it is necessary to use complete expression (33), (34) for $U_{\text{eff}}(\mathbf{p}, \mathbf{q})$ and not reduced expression (32). With such an approach, the polarization effects proportional to UV and V^2 considerably modify and complicate the structure of the phase diagram (Fig. 6a) even for small values of V_1. With increasing parameter V_1 of the intersite Coulomb interaction, the value of $|\lambda|$ for $T_c \sim W\exp(-1/|\lambda|)$ increases ($W = 8t_1$ is the 2D bandwidth for $t_2 = t_3 = 0$). In this case, only the three phases corresponding to the d_{xy}-wave, p-wave, and s-wave types of symmetry of the superconducting order parameter are stabilized. It should be noted that in the range of high electron concentrations and for $0.25 < V_1/|t_1| < 0.5$, the Kohn–Luttinger polarization effects lead to the occurrence of the superconducting s-wave phase. This qualitative effect visually demonstrates the importance of taking into account the second-order processes in calculating the effective interaction of electrons in the Cooper channel and in constructing the phase diagram in Fig. 6. Quantitative comparison of various partial contributions to the total effective interaction shows that s-wave pairing is associated with the polarization contributions proportional to V^2; the main contribution in this case for a square lattice is determined by the angular harmonic

$$g_1^{(s)}(\phi) = \frac{1}{\sqrt{\pi}}\cos 4\phi.$$

Such a scenario of achieving superconducting s-wave pairing due to higher angular harmonics correlates well with the experimental data obtained recently in [69], in which the results of investigating a superconductor based on iron arsenide KFe_2As_2 using photoemission spectroscopy with ultrahigh angular resolution were presented. It was found that this compound is a nodal (containing gap zeros) superconductor with the s-wave type symmetry of the order parameter, which has eight points at which the gap vanishes.

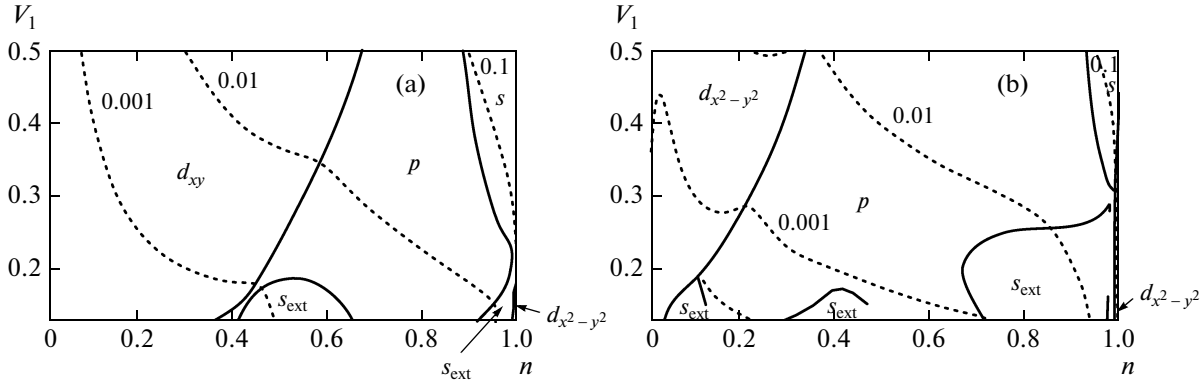

Fig. 6. Phase diagram in the Shubin–Vonsovsky model, constructed taking into account the second-order contributions in V for the set of parameters $t_2 = t_3 = 0$, $U = |t_1|$ and for the ratios $V_2/V_1 = 0$ (a) and 0.5 (b). Dotted curves show the lines of constant values of λ.

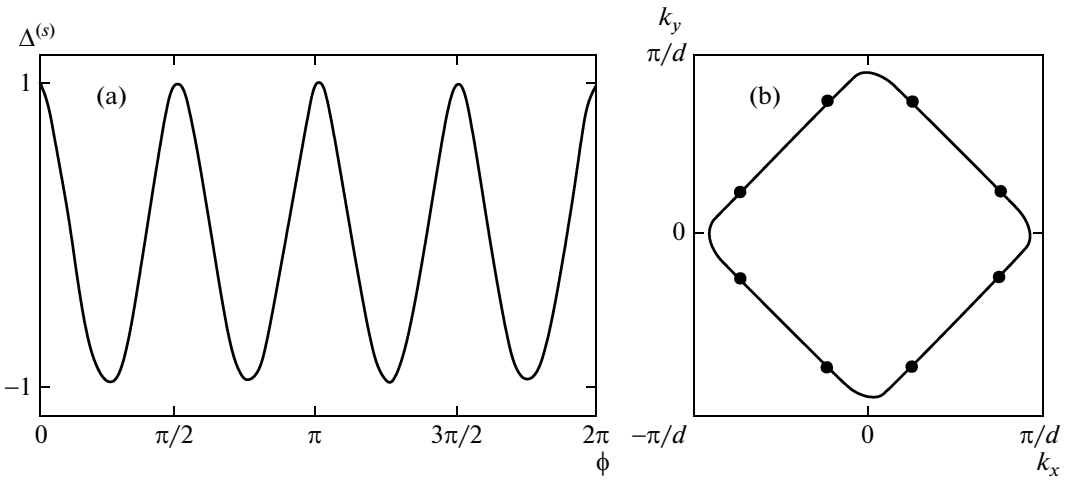

Fig. 7. (a) Angular dependence of superconducting order parameter $\Delta^{(s)}(\phi)$ and (b) positions of nodal points at which $\Delta^{(s)}(\phi)$ vanishes on the Fermi contour, calculated for parameters $t_2 = t_3 = 0$, $U = |t_1|$, $V_1 = 0.5|t_1|$, $V_2 = 0$, and $n = 0.95$.

Figure 7a shows the angular dependence of the superconducting order parameter $\Delta^{(s)}(\phi)$,

$$\Delta^{(s)}(\phi) = \frac{\Delta_0^{(s)}}{\sqrt{2}} + \Delta_1^{(s)}\cos 4\phi + \Delta_2^{(s)}\cos 8\phi + \Delta_3^{(s)}\cos 12\phi + \Delta_4^{(s)}\cos 16\phi, \quad (35)$$

calculated in [68] for the region of the phase diagram in which the *s*-wave pairing takes place for high electron densities. This dependence demonstrates the existence of the eight nodal points at which the gap vanishes; the position of these points on the Fermi contour (Fig. 7b) in calculations [68] is in qualitative agreement with the picture described in [69].

An analogous scenario of superconductivity realization is also observed in the *p*-wave channel; in this case, superconductivity obtained taking into account the second order of perturbation theory in the Coulomb interaction is suppressed by the initial repulsion only for the first harmonic:

$$g_0^{(p)}(\phi) = \frac{1}{\sqrt{\pi}}(A\sin\phi + B\cos\phi).$$

The main contribution to $\Delta^{(p)}(\hat{\mathbf{p}})$ comes from the function of the next harmonic of *p*-wave pairing:

$$g_1^{(p)}(\phi) = \frac{1}{\sqrt{\pi}}(A\sin 3\phi + B\cos 3\phi).$$

The effect of the long-range Coulomb repulsion ($V_2 \neq 0$) and distant electron hoppings ($t_2 \neq 0$, $t_3 \neq 0$) on the phase diagram of the superconducting state in the Shubin–Vonsovsky model was also analyzed in [68]. Figure 8 shows the modification of the phase diagram of the Shubin–Vonsovsky model, which is observed upon an increase in Hubbard repulsion parameter *U*. It can be seen that in the range of low electron densities, as well as in the range of densities close to the Van Hove singularity, the superconducting phase with the $d_{x^2-y^2}$-wave symmetry of the order parameter is achieved with quite large values of $|\lambda| \sim 0.1$–0.2. This result is important for analyzing the possibility of achieving the Kohn–Luttinger mechanism in high-T_c superconductors. It should be noted that for $|\lambda| \sim 0.2$, the superconducting transition temperatures can reach the values $T_c^{d_{x^2-y^2}} \sim 100$ K, which are realistic for curates.

5. *t–J* MODEL

After Anderson formulated his idea [2] that the electronic properties of cuprate superconductors can be described by the Hubbard model in the strong-coupling limit ($U \gg W$), the so-called *t–J* model has become extremely popular. The Hamiltonian of the *t–J* model with a released constraint has the form [70]

$$\hat{H} = \sum_{f\sigma}(\varepsilon - \mu)c_{f\sigma}^{\dagger}c_{f\sigma} + \sum_{fm\sigma} t_{fm}c_{f\sigma}^{\dagger}c_{m\sigma} + U\sum_f \hat{n}_{f\uparrow}\hat{n}_{f\downarrow} + \frac{1}{2}\sum_{\langle fm\rangle} J_{fm}\left(\mathbf{S}_f\mathbf{S}_m - \frac{\hat{n}_f\hat{n}_m}{4}\right). \quad (36)$$

In fact, it is a model with a strong Coulomb repulsion between electrons at the same site and with a weak antiferromagnetic interaction $J > 0$ at neighboring sites. Thus, the hierarchy of the model parameters has the form $U \gg \{J, t\}$. The phase diagram of the *t–J* model constructed in [70] is shown in Fig. 9.

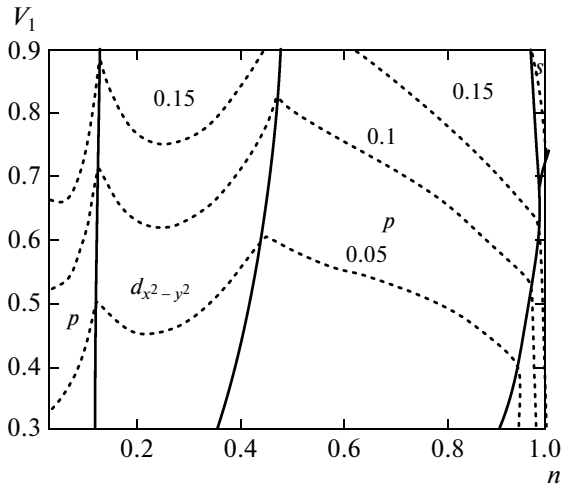

Fig. 8. Phase diagram in the Shubin–Vonsovsky model, obtained for parameters $t_2 = 0.15|t_1|$, $t_3 = 0.1|t_1|$, $U = 2|t_1|$, and $V_2/V_1 = 0.5$. Dotted curves are the lines of constant value of λ.

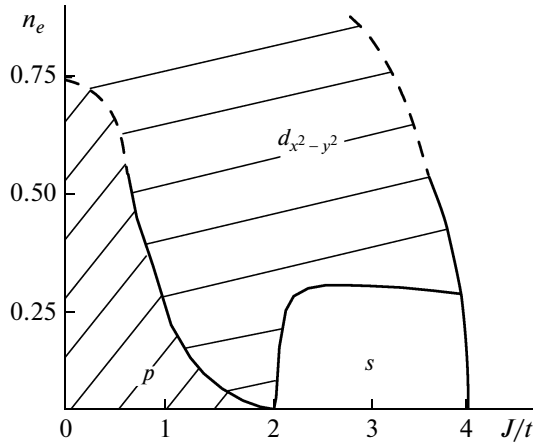

Fig. 9. Phase diagram of the superconducting state in the 2D t–J model for small and intermediate values of electron density.

For the realistic parameters of optimally doped cuprate superconductors ($J/t \sim 0.5$, $n = 2\varepsilon_F/W = 0.85$), we can obtain the following estimate for the superconducting transition temperature:

$$T_c^{d_{x^2-y^2}} \sim \varepsilon_F \exp\left(-\frac{\pi t}{2Jn^2}\right) \sim 10^2 \text{ K}. \quad (37)$$

It is important that an analogous estimate of the superconducting transition temperature for the $d_{x^2-y^2}$-wave pairing was obtained in [71] using a more rigorous theory for optimally doped cuprates by employing the Hubbard operator technique.

It should be noted that the development of the Kohn–Luttinger ideology for the strong-coupling regime for a nearly half-filling has become one of the most topical trends in the theory of superconductivity in strongly correlated systems. However, the solution of this problem requires taking into account strong single-site correlations in all orders of perturbation theory. The intersite correlations should be described with allowance for second-order contributions. One of the scenarios of the development of the theory is associated with the use of the atomic representation [72] and diagram technique for the Hubbard operators [73]. The models in which the Kohn–Luttinger renormalizations can be taken into account include the generalized t–J–V model [74–76] and the t–J^*–V model with three-center interactions (the important role of such interactions in describing the superconducting state was studied in [77–84]). These models are effective low-energy versions of the Shubin–Vonsovsky model.

6. IDEALIZED MONOLAYER OF DOPED GRAPHENE

The popularity of the Kohn–Luttinger mechanism continues to increase due to its possible implementation in other important physical systems. For example, the conditions of its occurrence in topological superfluid liquids [85], as well as in an idealized doped graphene monolayer, in which the effect of nonmagnetic impurities and the Van der Waals potential of the substrate are disregarded, are being actively discussed at present.

One of the most interesting properties of graphene is associated with the possibility of controlling the position of the chemical potential in this material by applying an electric field and, hence, by changing the type of charge carriers (electrons or holes). It was shown experimentally [86] that short graphene samples can be used to construct Josephson junctions by placing them between superconducting contacts. This means that Cooper pairs can propagate coherently in graphene. This result suggests that graphene can probably be modified structurally or chemically so that it becomes a magnet [87] or even a real superconductor.

It is known that, theoretically, the model with conical dispersion requires the minimal intensity of the pairing interaction for the development of Cooper instability [88]. In this connection, several attempts have been made to theoretically analyze the possibility of the superconducting state in doped graphene. The role of topological defects in Cooper pairing in this material was studied in [89]. In [90], a phase diagram was obtained in the mean-field approximation for the spin-singlet superconductivity in graphene; the plasmon superconductivity mechanism leading to low superconducting transition temperatures in the s-wave channel was investigated for realistic values of electron concentrations. The possibility of inducing supercon-

ductivity in graphene by electron correlations was investigated in [91, 92]. In [93], the functional renormalization group method was employed to study the competition between the superconducting phase with the $d + id$ symmetry type of the order parameter and the phase of the spin density wave on the Van Hove singularity in the density of electron states of graphene. In the vicinity of the Van Hove singularity, superconducting phases with the $d + id$-wave and f-wave types of the order parameter symmetry were found.

In [94], the situation was considered with the Fermi level near one of the Van Hove singularities in the density of states of graphene. It is well known that these singularities can enhance magnetic and superconducting fluctuations [95]. According to the scenario described in [94], the Cooper instability appears due to anisotropy of the Fermi contour for Van Hove filling n_{vH}, which in fact is related to the Kohn–Luttinger mechanism. It was noted [94] that the implementation of this mechanism in graphene is possible because the electron–electron scattering becomes strongly anisotropic and, hence, a channel with attraction may appear for some harmonics with a nontrivial angular dependence on the Fermi surface. Such a Cooper instability in an idealized graphene monolayer can ensure superconducting transition temperatures up to $T_c \sim 1$ K depending on the ability to tune the chemical potential level to the Van Hove singularity to the greatest possible extent. It should be noted that only the Coulomb repulsion of electrons at one site was taken into account in calculations. As mentioned above, the existence of the Van der Waals potential of the substrate and nonmagnetic impurities were ignored.

The possibility of competition and coexistence of the Pomeranchuk instability and the Kohn–Luttinger superconducting instability in graphene was considered in [96]. In [97–99], it was shown by the Kohn–Luttinger mechanism that chiral superconductivity of the $d + id$-wave type can be achieved in a doped graphene monolayer. Using the renormalization group method, the authors of [97–99] in fact proved that the Cooper instability evolves simultaneously in two degenerate d-wave channels.

Our recent publication [100] was devoted to analyzing Kohn–Luttinger superconductivity in an idealized doped graphene monolayer taking into account the Coulomb repulsion of electrons on the same and nearest carbon atoms in the Born weak coupling approximation. The necessity of taking into account the long-range Coulomb interaction in calculating the physical characteristics was dictated by the results of recent work [101], in which the partly screened frequency-dependent Coulomb interaction was calculated ab initio in constructing the effective many-body model of graphene and graphite. It was found that the one-atomic repulsion in graphene amounts to $U = 9.3$ eV, which contradicts the intuitively predicted small value of U and weak coupling ($U < W$). Calculations demonstrated the fundamental importance of taking into account nonlocal Coulomb interaction in graphene because the Coulomb repulsion of electrons located at neighboring sites is $V = 5.5$ eV according to ab initio calculations [101]. It should be noted that other researchers consider the value of V to be much smaller.

In the hexagonal lattice of graphene, each unit cell corresponds to two carbon atoms; therefore, the entire lattice can be split into two sublattices A and B. The Hamiltonian of the Shubin–Vonsovsky model for graphene, which takes into account electrons hoppings between the nearest and next-to-nearest atoms, as well as the Coulomb repulsion of electrons on the same and on neighboring atoms, has the following form in the Wannier representations:

$$\hat{H} = \hat{H}_0 + \hat{H}_{\text{int}}, \tag{38}$$

where in the real space

$$\hat{H}_0 = -\mu\sum_f(\hat{n}_f^A + \hat{n}_f^B) - t_1\sum_{\langle fm\rangle\sigma}(a_{f\sigma}^\dagger b_{m\sigma} + \text{H.c.}) - t_2\sum_{\langle\langle fm\rangle\rangle\sigma}(a_{f\sigma}^\dagger a_{m\sigma} + b_{f,\sigma}^\dagger b_{m,\sigma} + \text{H.c.}), \tag{39}$$

$$\hat{H}_{\text{int}} = U\sum_f(\hat{n}_{f\uparrow}^A\hat{n}_{f\downarrow}^A + \hat{n}_{f\uparrow}^B\hat{n}_{f\downarrow}^B) + V\sum_{\langle fm\rangle}\hat{n}_f^A\hat{n}_m^B. \tag{40}$$

Operators $a_{f\sigma}^\dagger$ ($a_{f\sigma}$) in expressions (39) and (40) create (annihilate) an electron with spin projection $\sigma = \pm 1/2$ at site f of sublattice A. At the same time, expression

$$\hat{n}_f^A = \sum_\sigma \hat{n}_{f\sigma}^A = \sum_\sigma a_{f\sigma}^\dagger a_{f\sigma}$$

denotes the operator of fermion density at site f of sublattice A (analogous notation can be used for sublattice B). In Hamiltonian (38)–(40), angle brackets $\langle\ldots\rangle$ indicate that the summation is carried out only over the nearest neighbors, while $\langle\langle\ldots\rangle\rangle$ indicates that the summation is performed over the next-to-nearest neighbors.

Passing to the momentum space and performing the Bogoliubov $u-v$ transformation,

$$\begin{aligned} a_{\mathbf{k}\sigma} &= w_{\mathbf{k}}\alpha_{\mathbf{k}\sigma} + z_{\mathbf{k}}\beta_{\mathbf{k}\sigma}, \\ b_{\mathbf{k}\sigma} &= w_{\mathbf{k}}^*\beta_{\mathbf{k}\sigma} - z_{\mathbf{k}}^*\alpha_{\mathbf{k}\sigma}, \end{aligned} \tag{41}$$

where $\alpha_{\mathbf{k}\sigma}$ and $\beta_{\mathbf{k}\sigma}$ are the operators describing the dynamics of electrons in the upper and lower bands of graphene, we can diagonalize Hamiltonian $\hat{H}_0$. The interacting part $\hat{H}_{\text{int}}$ of the Hamiltonian was written in [100] in the representation of Bogoliubov operators (41); we derived the expression for the effective interaction of electrons taking into account the polarization contributions described by the diagrams in Fig. 2.

The possibility of Cooper pairing is determined by the characteristics of the energy spectrum in the vicin-

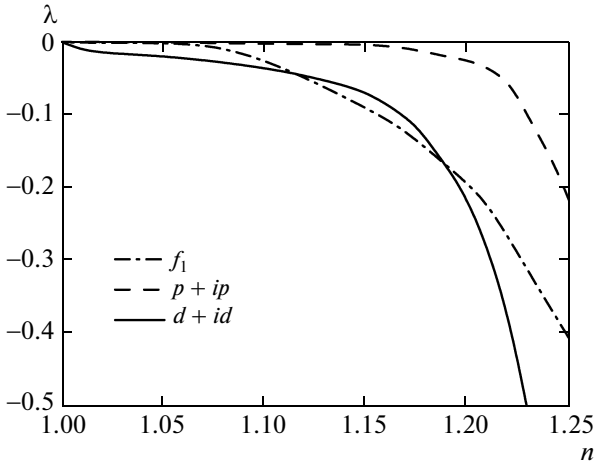

Fig. 10. Dependence of λ on carrier concentration n taking into account the effective interaction of electrons with energies corresponding to both branches of the graphene spectrum for $t_2 = 0.2|t_1|$, $U = 3|t_1|$, and $V = 0.5|t_1|$; $t_1 = 1$, $t_2 = 0.2$, $U = 3$, $V = 0.5$.

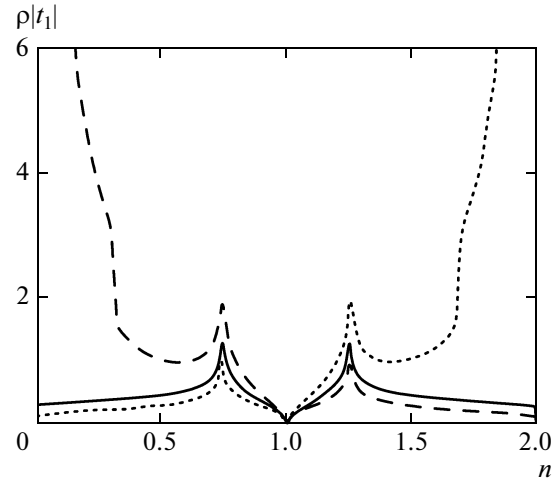

Fig. 11. Modification of the electron density of states in graphene with the inclusion of hoppings to the next-to-nearest atoms for $t_2 = -0.2|t_1|$ (dashed curve), $t_2 = 0$ (solid curve), $t_2 = 0.2|t_1|$ (dotted curve).

ity of the Fermi level and by the effective interaction of electrons near the Fermi surface [21]. We assumed in [100] that upon doping of graphene, the chemical potential gets into the upper band; accordingly, in analyzing the conditions for anomalous pairing, we considered the polarization contributions associated with the Coulomb interaction of electrons with energies corresponding to only one or both branches of the energy spectrum of graphene (both Dirac cones).

Figure 10 shows the dependences of the effective coupling constant on the electron concentration, which were obtained taking into account the effective interaction of electrons with the energies corresponding to both branches of the graphene energy spectrum for the set of parameters $t_2 = 0.2|t_1|$, $U = 3|t_1|$, and $V = 0.5|t_1|$. It can be seen that for electron densities $1 < n < 1.13$, competition appears between superconducting phase of the $d + id$-wave type of the order parameter symmetry, which are described by 2D representation E_2, and the superconducting phase with the f-wave type of symmetry. For electron concentrations $1.18 < n < 1.25$, the ground state of the system corresponds to the superconducting phase with the $d + id$-wave type symmetry of order parameter.

Analysis carried out in [100] revealed that the inclusion of electron hoppings to next-to-nearest carbon atoms (t_2) does not qualitatively affect the competition between superconducting phases. Such a behavior of the system can be explained by the fact that activation of hoppings $t_2 > 0$ or $t_2 < 0$ leads to only a quantitative change in the electron density of states in graphene, but does not affect its dependence on the carrier concentration (Fig. 11). As a result, allowance for distant hoppings in t_2 leads to an increase in the absolute values of the effective interaction and, hence, to a higher superconducting transition temperature in doped graphene [100].

The possibility of Cooper pairing in graphene was analyzed in [102] in the opposite strong-coupling limit $U \gg t$ on the basis of the kinematic mechanism of superconductivity using the diagram technique for the Hubbard operators [49, 73]. As mentioned above, the feasibility of the strong-coupling limit for graphene was announced in [101].

7. CONCLUSIONS

In this review, we have demonstrated the instability of the normal state of a repulsive electron gas and of electron systems on the lattice to the transition to the superconducting phase in accordance with the Kohn–Luttinger mechanism for various electron models. The initial conclusion concerning Cooper instability for the model of a repulsive Fermi gas with a quadratic dispersion relation was generalized for electrons in real crystalline solids considered in the tight binding approximation. The difference between the dispersion relation for electrons from the quadratic law leads to a number of additional peculiarities associated with the effects of the Brillouin zone. For example, it turned out that the form of the electron energy spectrum determined by hopping parameters affects the concentration dependence of the superconducting transition temperature as well as the order parameter symmetry. As a result, there is a change in the structure of the phase diagram that determines the regions of achievement of superconducting phases with different types of the order parameter symmetry. However, the conclusion concerning the possibility of Cooper instability with the Kohn–Luttinger mechanism in the

electron plasma in the tight binding approximation generally holds.

In this review, it was illustrated that the universal nature of the Kohn–Luttinger mechanism is preserved even if we take into account the finiteness of the screening radius in repulsive Fermi systems. At the same time, investigations based on the Shubin–Vonsovsky model demonstrated that it is important to take into account the Coulomb repulsion of electrons at different sites of crystal lattice. In this case, the phase diagram of the superconducting state changes, and the superconducting transition temperature can be increased under certain conditions.

We also showed that the Kohn–Luttinger mechanism of superconducting pairing can be realized in systems with a linear dispersion relation. This was demonstrated for an idealized graphene monolayer possessing a hexagonal lattice with two carbon atoms per unit cell. It was shown that the polarization effects in such a system lead to an effective attraction in the Cooper channel.

The above arguments lead to the conclusion about the universal nature of the Kohn–Luttinger mechanism for the formation of Cooper instability in repulsive Fermi systems and for superconducting pairing with a nonzero orbital angular momentum. It should also be noted that in many cases this mechanism leads to quite high superconducting transition temperatures (as shown in [40], especially in the two-band situation with a wide and a narrow band). Moreover, for electron concentrations close to the Van Hove singularity in the electron density of states, the superconducting transition temperatures increase still further and may reach the values of the order of 100 K even in the one-band case for intermediate values of the ratio of the Hubbard repulsion parameter to the conduction band width (U/W).

ACKNOWLEDGMENTS

The authors are grateful to the late A.S. Aleksandrov, D.V. Efremov, V.V. Kabanov, the late Yu.V. Kopaev, K.I. Kugel, M.S. Mar'enko, N.M. Plakida, and A.V. Chubukov for numerous discussions and unceasing interest in this research.

This study was supported by the Program of the Physics Department of the Russian Academy of Sciences (project no. P.3.1) and the Russian Foundation for Basic Research (project nos. 14-02-00058 and 14-02-31237). The work of two coauthors (M.M.K. and V.A.M) was supported financially by grant no. MK-526.2013.2 of the President of the Russian Federation and the Dynasty Foundation.

REFERENCES

1. J. Bardeen, L. N. Cooper, and J. R. Schrieffer, Phys. Rev. **108**, 1175 (1957).
2. P. W. Anderson, Science (Washington) **235**, 1196 (1987).
3. D. Vollhardt and P. Woelfle, *The Superfluid Phases of Helium 3* (Taylor and Francis, London, 1990).
4. G. E. Volovik, *Exotic Properties of Superfluid ^3He* (World Scientific, Singapore, 1992).
5. G. E. Volovik, *The Universe in a Helium Droplet* (Clarendon, Oxford, 2003).
6. C. A. Regal, C. Ticknor, J. L. Bohn, and D. S. Jin, Phys. Rev. Lett. **90**, 053201 (2003).
7. C. H. Schunck, M. W. Zwierlein, C. A. Stan, S. M. F. Raupach, W. Ketterle, A. Simoni, E. Tiesinga, C. J. Williams, and P. S. Julienne, Phys. Rev. A: At., Mol., Opt. Phys. **71**, 045601 (2005).
8. H. R. Ott, H. Rudigier, T. M. Rice, K. Ueda, Z. Fisk, and J. L. Smith, Phys. Rev. Lett. **52**, 1915 (1984).
9. S. Kromer, R. Helfrich, M. Lang, F. Steglich, C. Langhammer, A. Bach, T. Michels, J. S. Kim, and G. R. Stewart, Phys. Rev. Lett. **81**, 4476 (1998).
10. K. Kuroki, J. Phys. Soc. Jpn. **75**, 051013 (2006).
11. Y. Maeno, T. M. Rice, and M. Sigrist, Phys. Today **54**, 42 (2001); T. M. Rice and M. Sigrist, J. Phys.: Condens. Matter **7**, L643 (1995).
12. J. Nagamatsu, N. Nakagawa, T. Muranaka, Y. Zenitani, and J. Akimitsu, Nature (London) **410**, 63 (2001).
13. Y. Kamihara, T. Watanabe, M. Hirano, and H. Hosono, J. Am. Chem. Soc. **130**, 3296 (2008).
14. K. S. Novoselov, A. K. Geim, S. V. Morozov, D. Jiang, Y. Zhang, S. V. Dubonos, I. V. Grigorieva, and A. A. Firsov, Science (Washington) **306**, 666 (2004).
15. M. Yu. Kagan, Phys.—Usp. **37** (1), 69 (1994).
16. Yu. E. Lozovik, S. P. Merkulova, and A. A. Sokolik, Phys.—Usp. **51** (7), 727 (2008).
17. V. N. Kotov, B. Uchoa, V. M. Pereira, F. Guinea, and A. H. Castro Neto, Rev. Mod. Phys. **84**, 1067 (2012).
18. P. R. Wallace, Phys. Rev. **71**, 622 (1947).
19. A. H. Castro Neto, F. Guinea, N. M. R. Peres, K. S. Novoselov, and A. K. Geim, Rev. Mod. Phys. **81**, 109 (2009).
20. W. Kohn and J. M. Luttinger, Phys. Rev. Lett. **15**, 524 (1965).
21. L. P. Gor'kov and T. K. Melik-Barkhudarov, Sov. Phys. JETP **13**, 1018 (1961).
22. J. Friedel, Adv. Phys. **3**, 446 (1954); J. Friedel, Nuovo Cimento, Suppl. **2**, 287 (1958).
23. J. Lindhard and K. Dan, Vidensk. Selsk. Mat.–Fys. Medd. **28**, 8 (1954).
24. N. Ashcroft and N. Mermin, *Solid State Physics* (Holt, Rinehart and Winston, New York, 1976; Mir, Moscow, 1979), Vol. 1.
25. A. B. Migdal, Sov. Phys. JETP **7**, 996 (1958).
26. W. Kohn, Phys. Rev. Lett. **2**, 393 (1959).
27. D. Fay and A. Layzer, Phys. Rev. Lett. **20**, 187 (1968).
28. M. Yu. Kagan and A. V. Chubukov, JETP Lett. **47** (10), 614 (1988).
29. M. A. Baranov, A. V. Chubukov, and M. Yu. Kagan, Int. J. Mod. Phys. B **6**, 2471 (1992).

30. M. A. Baranov, M. Yu. Kagan, and Yu. Kagan, JETP Lett. **64** (4), 301 (1996).
31. V. M. Galitskii, Sov. Phys. JETP **7**, 104 (1958).
32. M. Yu. Kagan and A. V. Chubukov, JETP Lett. **50** (11), 517 (1989).
33. A. V. Chubukov, Phys. Rev. B: Condens. Matter **48**, 1097 (1993).
34. D. V. Efremov, M. S. Mar'enko, M. A. Baranov, and M. Yu. Kagan, Physica B (Amsterdam) **284–288**, 216 (2000).
35. P. Bloom, Phys. Rev. B: Solid State **12**, 125 (1975).
36. A. M. Afanas'ev and Yu. Kagan, Sov. Phys. JETP **16**, 1030 (1962).
37. D. V. Efremov, M. S. Mar'enko, M. A. Baranov, and M. Yu. Kagan, JETP **90** (5), 861 (2000).
38. G.-H. Oh, Y. Ishimoto, T. Kawae, M. Nakagawa, O. Ishikawa, T. Hata, and T. Kodama, J. Low Temp. Phys. **95**, 525 (1994).
39. M. Yu. Kagan, Phys. Lett. A **152**, 303 (1991).
40. M. Yu. Kagan and V. V. Val'kov, J. Exp. Theor. Phys. **113** (1), 156 (2011); M. Yu. Kagan and V. V. Val'kov, Low Temp. Phys. **37** (1), 69 (2011); G. Lanzarich, *Lifetime in Magnetism and Superconductivity: A Tribute to Professor David Schoenberg* (Cambridge Scientific, Cambridge, 2011).
41. M. Yu. Kagan, V. V. Val'kov, and P. Woelfle, Low Temp. Phys. **37** (10), 834 (2011).
42. M. A. Baranov, M. Yu. Kagan, and M. S. Mar'enko, JETP Lett. **58** (9), 709 (1993).
43. J. G. Bednorz and K. A. Müller, Z. Phys. B: Condens. Matter **64**, 189 (1986).
44. J. C. Hubbard, Proc. R. Soc. London, Ser. A **276**, 238 (1963).
45. Yu. A. Izyumov, M. I. Katsnel'son, and Yu. N. Skryabin, *Magnetism of Itinerant Electrons* (Nauka, Moscow, 1994) [in Russian].
46. Yu. A. Izyumov, Phys.—Usp. **38** (4), 385 (1995).
47. A. Georges, G. Kotliar, W. Krauth, and M. J. Rozenberg, Rev. Mod. Phys. **68**, 13 (1996).
48. H. Tasaki, J. Phys.: Condens. Matter. **68**, 4353 (1998).
49. S. G. Ovchinnikov and V. V. Val'kov, *Hubbard Operators in the Theory of Strongly Correlated Electrons* (Imperial College Press, London, 2004).
50. M. A. Baranov and M. Yu. Kagan, Z. Phys. B: Condens. Matter **86**, 237 (1992).
51. L. D. Landau and E. M. Lifshitz, *Course of Theoretical Physics*, Volume 3: *Quantum Mechanics: Non-Relativistic Theory* (Nauka, Moscow, 1989; Butterworth–Heinemann, Oxford, 1991).
52. D. J. Scalapino, E. Loh, Jr., and J. E. Hirsch, Phys. Rev. B: Condens. Matter **34**, 8190 (1986); D. J. Scalapino, E. Loh, Jr., and J. E. Hirsch, Phys. Rev. B: Condens. Matter **35**, 6694 (1987).
53. A. N. Kozlov, Sverkhprovodimost: Fiz., Khim., Tekh. **2**, 64 (1989).
54. R. Hlubina, Phys. Rev. B: Condens. Matter **59**, 9600 (1999); J. Mráz and R. Hlubina, Phys. Rev. B: Condens. Matter **67**, 174518 (2003).
55. D. Zanchi and H. J. Schulz, Phys. Rev. B: Condens. Matter **54**, 9509 (1996).
56. I. E. Dzyaloshinskii and V. M. Yakovenko, Sov. Phys. JETP **67** (4), 844 (1988); I. E. Dzyaloshinskii, I. M. Krichever, and J. Chronek, Sov. Phys. JETP **67** (7), 1492 (1988).
57. A. T. Zheleznyak, V. M. Yakovenko, and I. E. Dzyaloshinskii, Phys. Rev. B: Condens. Matter **55**, 3200 (1997).
58. S. Raghu, S. A. Kivelson, and D. J. Scalapino, Phys. Rev. B: Condens. Matter **81**, 224505 (2010).
59. A. S. Alexandrov and V. V. Kabanov, Phys. Rev. Lett. **106**, 136403 (2011).
60. S. Shubin and S. Vonsovsky, Proc. R. Soc. London, Ser. A **145**, 159 (1934); S. Shubin and S. Vonsovsky, Phys. Z. Sowjetunion **7**, 292 (1935); S. Shubin and S. Vonsovsky, Phys. Z. Sowjetunion **10**, 348 (1936).
61. S. V. Vonsovsky and M. I. Katsnelson, J. Phys. C: Solid State Phys. **12**, 2043 (1979); S. V. Vonsovsky and M. I. Katsnelson, J. Phys. C: Solid State Phys. **12**, 2055 (1979).
62. R. O. Zaitsev, Sov. Phys. JETP **51** (4), 671 (1980).
63. R. O. Zaitsev, V. A. Ivanov, and Yu. V. Mikhailova, Fiz. Met. Metalloved. **65**, 1032 (1988); R. O. Zaitsev, V. A. Ivanov, and Yu. V. Mikhailova, Fiz. Met. Metalloved. **65**, 1108 (1989).
64. R. O. Zaitsev, J. Exp. Theor. Phys. **98** (4), 780 (2004).
65. V. V. Val'kov and M. M. Korovushkin, J. Exp. Theor. Phys. **112** (1), 108 (2011).
66. M. Yu. Kagan, D. V. Efremov, M. S. Mar'enko, and V. V. Val'kov, JETP Lett. **93** (12), 725 (2011).
67. S. Raghu, E. Berg, A. V. Chubukov, and S. A. Kivelson, Phys. Rev. B: Condens. Matter **85**, 024516 (2012).
68. M. Yu. Kagan, V. V. Val'kov, V. A. Mitskan, and M. M. Korovushkin, JETP Lett. **97** (4), 226 (2013); M. Yu. Kagan, V. V. Val'kov, V. A. Mitskan, and M. M. Korovushkin, J. Exp. Theor. Phys. **117** (4), 728 (2013).
69. K. Okazaki, Y. Ota, Y. Kotani, W. Malaeb, Y. Ishida, T. Shimojima, T. Kiss, S. Watanabe, C.-T. Chen, K. Kihou, C. H. Lee, A. Iyo, H. Eisaki, T. Saito, H. Fukazawa, Y. Kohori, K. Hashimoto, T. Shibauchi, Y. Matsuda, H. Ikeda, H. Miyahara, R. Arita, A. Chainani, and S. Shin, Science (Washington) **337**, 1314 (2012).
70. M. Yu. Kagan and T. M. Rice, J. Phys.: Condens. Matter **6**, 3771 (1994).
71. N. M. Plakida, JETP Lett. **74** (1), 36 (2001); N. M. Plakida, L. Anton, S. Adam, and Gh. Adam, J. Exp. Theor. Phys. **97** (2), 331 (2003).
72. J. C. Hubbard, Proc. R. Soc. London, Ser. A **285**, 542 (1965).
73. R. O. Zaitsev, Sov. Phys. JETP **41** (1), 100 (1975); R. O. Zaitsev, Sov. Phys. JETP **43** (3), 574 (1976).
74. M. Eremin, I. Eremin, and S. Varlamov, Phys. Rev. B: Condens. Matter **64**, 214512 (2001).
75. M. V. Eremin, I. M. Shigapov, and I. M. Eremin, Eur. Phys. J. B **85**, 131 (2012).
76. N. M. Plakida and V. S. Oudovenko, Eur. Phys. J. B **86**, 115 (2013).
77. J. E. Hirsch, Phys. Lett. A **136**, 153 (1989).
78. V. Yu. Yushankhai, G. M. Vujicic, and R. B. Zakula, Phys. Lett. A **151**, 254 (1990).

79. V. V. Val'kov, T. A. Val'kova, D. M. Dzebisashvili, and S. G. Ovchinnikov, Mod. Phys. Lett. B **17**, 441 (2003).
80. V. V. Val'kov and D. M. Dzebisashvili, J. Exp. Theor. Phys. **100** (3), 608 (2005).
81. M. M. Korshunov, S. G. Ovchinnikov, and A. V. Sherman, JETP Lett. **80** (1), 39 (2004).
82. V. V. Val'kov and A. A. Golovnya, J. Exp. Theor. Phys. **107** (6), 996 (2008).
83. V. V. Val'kov, M. M. Korovushkin, and A. F. Barabanov, JETP Lett. **88** (6), 370 (2008).
84. V. V. Val'kov, A. A. Shklyaev, M. M. Korovushkin, and A. F. Barabanov, Phys. Solid State **53** (10), 1997 (2011).
85. M. S. Mar'enko, J. D. Sau, and S. Tewari, arXiv:1202.5784v1.
86. H. B. Heersche, P. Jarillo-Herrero, J. B. Oostinga, L. M. K. Vandersypen, and A. F. Morpurgo, Nature (London) **446**, 56 (2007).
87. N. M. R. Peres, F. Guinea, and A. H. Castro Neto, Phys. Rev. B: Condens. Matter **72**, 174406 (2005).
88. E. C. Marino and L. H. C. M. Nunes, Nucl. Phys. B **741**, 404 (2006).
89. J. González, F. Guinea, and M. A. H. Vozmediano, Phys. Rev. B: Condens. Matter **63**, 134421 (2001).
90. B. Uchoa and A. H. Castro Neto, Phys. Rev. Lett. **98**, 146801 (2007).
91. A. M. Black-Schaffer and S. Doniach, Phys. Rev. B: Condens. Matter **75**, 134512 (2007).
92. C. Honerkamp, Phys. Rev. Lett. **100**, 146404 (2008).
93. M. L. Kiesel, C. Platt, W. Hanke, D. A. Abanin, and R. Thomale, Phys. Rev. B: Condens. Matter **86**, 020507(R) (2012).
94. J. González, Phys. Rev. B: Condens. Matter **78**, 205431 (2008).
95. R. S. Markiewicz, J. Phys. Chem. Solids **58**, 1179 (1997).
96. B. Valenzuela and M. A. H. Vozmediano, New J. Phys. **10**, 113009 (2008).
97. R. Nandkishore, L. S. Levitov, and A. V. Chubukov, Nat. Phys. **8**, 158 (2012).
98. R. Nandkishore, G.-W. Chern, and A. V. Chubukov, Phys. Rev. Lett. **108**, 227204 (2012).
99. R. Nandkishore and A. V. Chubukov, Phys. Rev. B: Condens. Matter **86**, 115426 (2012).
100. M. Yu. Kagan, V. V. Val'kov, V. A. Mitskan, and M. M. Korovushkin, Solid State Commun. **118**, 61 (2014).
101. T. O. Wehling, E. Şaşoğlu, C. Friedrich, A. I. Lichtenstein, M. I. Katsnelson, and S. Blugel, Phys. Rev. Lett. **106**, 236805 (2011).
102. R. O. Zaitsev, JETP Lett. **94** (3), 206 (2011); R. O. Zaitsev, JETP Lett. **95** (7), 380 (2012).

Translated by N. Wadhwa